

**Mirror nucleon removal reactions in  $p$ -shell nuclei**

A. N. Kuchera <sup>1</sup>, D. Bazin,<sup>2,3</sup> T. Phan,<sup>1</sup> J. A. Tostevin,<sup>4</sup> M. Babo,<sup>5</sup> T. Baumann,<sup>2</sup> P. C. Bender,<sup>6</sup> M. Bowry,<sup>2</sup> J. Bradt,<sup>2,3</sup> J. Brown,<sup>7</sup> P. A. DeYoung,<sup>8</sup> B. Elman,<sup>2,3</sup> J. E. Finck,<sup>9</sup> A. Gade,<sup>2,3</sup> G. F. Grinyer,<sup>10</sup> M. D. Jones,<sup>2,3</sup> B. Longfellow,<sup>2,3</sup> E. Lunderberg,<sup>2,3</sup> T. H. Redpath,<sup>2,3,\*</sup> W. F. Rogers,<sup>11</sup> K. Stiefel,<sup>2,12</sup> M. Thoennessen,<sup>2,3,†</sup> D. Votaw,<sup>2,3</sup> D. Weisshaar,<sup>2</sup> K. Whitmore,<sup>2,3</sup> and R. B. Wiringa<sup>13</sup>

<sup>1</sup>*Department of Physics, Davidson College, Davidson, North Carolina 28035, USA*

<sup>2</sup>*National Superconducting Cyclotron Laboratory, Michigan State University, East Lansing, Michigan 48824, USA*

<sup>3</sup>*Department of Physics and Astronomy, Michigan State University, East Lansing, Michigan 48824, USA*

<sup>4</sup>*Department of Physics, University of Surrey, Guildford, Surrey GU2 7XH, United Kingdom*

<sup>5</sup>*Grand Accélérateur National d'Ions Lourds (GANIL), CEA/DSM-CNRS/IN2P3, Bvd Henri Becquerel, 14076 Caen, France*

<sup>6</sup>*Department of Physics and Applied Physics, University of Massachusetts Lowell, Lowell, Massachusetts 01854, USA*

<sup>7</sup>*Department of Physics, Wabash College, Crawfordsville, Indiana 47933, USA*

<sup>8</sup>*Department of Physics, Hope College, Holland, Michigan 49423, USA*

<sup>9</sup>*Department of Physics, Central Michigan University, Mount Pleasant, Michigan 48859, USA*

<sup>10</sup>*Department of Physics, University of Regina, Regina, Saskatchewan S4S 0A2, Canada*

<sup>11</sup>*Physics Department, Indiana Wesleyan University, Marion, Indiana 46953, USA*

<sup>12</sup>*Department of Chemistry, Michigan State University, East Lansing, Michigan 48824, USA*

<sup>13</sup>*Physics Division, Argonne National Laboratory, Argonne, Illinois 60439, USA*



(Received 24 November 2021; accepted 18 February 2022; published 11 March 2022)

Nucleon removal reactions have been shown to be an effective tool for studying the single particle structure of nuclei. This work continues efforts to experimentally probe and benchmark the reaction and structure models used to calculate the removal reaction cross sections when using microscopic nuclear structure inputs. Three different single nucleon removal reactions were performed, from  $p$ -shell nuclei with masses  $A = 7, 9$ , and  $10$ . The residual nuclei from the reactions were detected in coincidence with  $\gamma$  rays to determine partial cross sections to individual final states. The eikonal direct-reaction model is combined with overlap functions and residual nucleus densities from microscopic, variational Monte Carlo calculations to provide consistent nuclear structure input to the partial cross section calculations. Comparisons of measured and calculated cross sections, including for mirror reactions, are presented. The analysis of the partial cross sections leading to the ground states shows a similar behavior to the one observed from analyses of inclusive cross sections using shell model nuclear structure input: the theoretical description of the removal process is in better agreement with the data when removing weakly bound nucleons, than when removing well-bound ones. The two mirror reaction pairs presented here show consistent results between the respective members of the pairs. The results obtained for the population of the excited states, however, show a systematically different trend that appears connected to the structure part of the calculation. Additional cases are needed to better understand the respective roles of structure and dynamical effects in the deviations.

DOI: [10.1103/PhysRevC.105.034314](https://doi.org/10.1103/PhysRevC.105.034314)

**I. INTRODUCTION**

A longstanding challenge in using direct nuclear reactions to infer quantitative spectroscopic properties of nuclei is to validate the ability of the reaction and structure models used to reliably calculate absolute cross sections. In intermediate energy nucleon removal reactions, as in lower energy single-nucleon transfer reactions, each transition between a given

initial and final state is studied by comparing its measured partial cross section with that computed with a direct-reaction model that attempts to describe accurately the dominant reaction mechanism(s), combined with a spectroscopic factor and overlap function obtained from a structure model. One of the main issues with this approach is the different footings on which each of the two models, reaction and structure, may be based upon. A recent review article goes into great detail highlighting the different approaches, such as nucleon transfer, nucleon removal reactions or quasifree scattering, with their respective experimental and theoretical challenges [1].

In the case of single nucleon removal reactions, the eikonal direct-reaction model, see, e.g., Ref. [2], has been combined

\*Present address: Virginia State University, Petersburg, VA 23806, USA.

†Present address: American Physical Society, Ridge, NY 11961, USA.

with shell model spectroscopic factors to make such comparisons with measurements [3,4]. The range of energies at which measurements have been carried out is large, from the many measurements made in the 80 to 120 MeV/nucleon range, to the more recent ones performed with beams at 240 MeV/nucleon [5,6], and as high as as 2100 MeV/nucleon [7]. In the approach presented here, a strategy is applied where outputs of a microscopic nuclear structure model are used directly as inputs in the reaction model. In addition, the aim of this work is to compare cross sections between mirror nuclei pairs, both in the initial and final states, in an attempt to disentangle the structure and reaction components that make up the theoretical cross section, based on the assumption that the spectroscopic factors calculated for the mirror reactions are identical. In the case where the final nuclei have bound excited states, this requires the measurement of partial cross sections to individual states, via in-beam  $\gamma$ -ray detection.

The reaction mechanisms involved here are elastic and inelastic dissociation of the projectile nucleus in which the target nucleus remains in, or is excited from its ground-state, respectively. The relative importance of these two mechanisms has already been tested using dedicated experiments [8,9] that measured both the residual nucleus and the removed nucleon. In these tests, the proton removal reactions from the light projectile nuclei  ${}^9\text{C}$  and  ${}^8\text{B}$  were chosen so as to populate residual nuclei with no bound excited states; thus avoiding any final-state ambiguity or the need for  $\gamma$ -ray detection. The measured proportions of the cross section from the elastic and inelastic mechanisms were in excellent agreement with the eikonal-model predictions for the proton-removal reactions studied. However, no assessment was made there of the absolute removal cross sections, the sum of these two contributions.

To further probe the absolute cross sections, Grinyer *et al.* [10] performed a series of nucleon removal reactions on  $p$ -shell nuclei in which the inclusive cross sections to the bound states of the residual nuclei were measured. The important feature of that study was to take the two structure inputs required by the eikonal-model calculations, comprising (a) the removed nucleon wave function (overlap function), whose normalization gives the spectroscopic factor, and (b) the residual nucleus density, from fully microscopic variational Monte Carlo (VMC) model calculations [11–13]. However, due to the inclusive nature of the measurements, a comparison of partial (i.e., residue final-state-exclusive) cross sections for reactions between individual mirror final states was not possible. To enable this, we report a new experiment, made with multiple beam and residual nuclei combinations and with a high-efficiency  $\gamma$ -ray detector array, to determine the relative cross sections to each bound final state of the residue. When combined with the earlier inclusive cross section measurements for the same nuclei, the new results allow the extraction of absolute partial cross sections that can be compared between mirror reaction pairs and with the theoretical predictions using VMC nuclear structure input. Note that mirror reaction pairs were studied recently for more complex nuclei [14] with an emphasis on comparing the structure of the mirror residues, but the focus of this study is the comparison between measured and calculated removal cross sections

TABLE I. Secondary beams, desired residues, and beam energies used in the nucleon removal reactions studied in this work.

Beam	Residues	Energy [MeV/nucleon]
${}^7\text{Li}$	${}^6\text{He}$ , ${}^6\text{Li}$	80
${}^9\text{Li}$	${}^8\text{Li}$	80
${}^{10}\text{Be}$	${}^9\text{Li}$	80

using inputs from *ab-initio* structure calculations in the reaction model.

## II. EXPERIMENT

The experiment was performed at the Coupled Cyclotron Facility at the National Superconducting Cyclotron Laboratory (NSCL) [15]. A primary beam of  ${}^{16}\text{O}$  was accelerated to 150 MeV/nucleon and impinged on a beryllium production target in the A1900 fragment separator [16]. The A1900 was tuned to deliver different secondary beams with high purity to the experimental area. These beams and the desired reaction products are listed in Table I.

The secondary beams were focused onto a beryllium reaction target (376 mg/cm<sup>2</sup>) with an energy of 80 MeV/nucleon to undergo proton or neutron removal reactions. 170 of the 192 CsI(Na) CAESAR scintillators [17] surrounded the reaction target to detect  $\gamma$  rays from the de-excitation of the residual nuclei. The reaction products were deflected 43° from the beam axis by the Sweeper magnet, a 4 T m superconducting large-gap dipole magnet [18]. Magnetic shielding was installed between CAESAR and the Sweeper magnet to reduce the fringe fields from affecting the performance of the photomultipliers of CAESAR. Downstream from the Sweeper magnet, the focal plane box contained two tracking detectors, an ionization chamber, and a large area plastic scintillator that provided the master trigger for the data acquisition system. A schematic of the experimental setup is shown in Fig. 1. The trigger opened a gate which recorded the energies registered in CAESAR to measure the coincident  $\gamma$  rays with each detected charged particle. The atomic numbers of the reaction products were determined by their energy loss in the ionization chamber, shown in Fig. 2. To separate the isotopes for a given element, their position, angle, and time of flight were used to calculate a corrected time of flight as shown in Fig. 3.

Absolute cross sections can only be determined by counting the number of incoming particles and residues produced in the target. Due to technical issues related to the secondary beam profile and the determination of the acceptances of the Sweeper magnet, absolute cross sections could not be reliably extracted in this experiment. However, since  $\gamma$  rays were only recorded in coincidence with residues detected in the focal plane, the relative cross sections to different final states could still be determined by comparing the number of  $\gamma$  rays to the number of residues. Reaction calculations were performed confirming that the difference in the momentum distributions from the ground state and excited states does not deviate more than the spread caused by energy loss in the target and the incoming beam momentum spread. It is therefore safe to

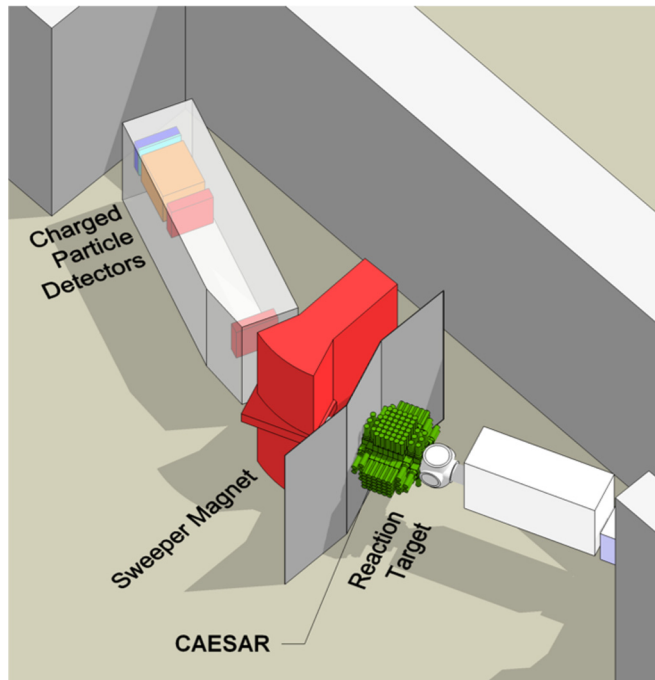


FIG. 1. Schematic of the experimental setup at NSCL. The beam is focused on the reaction target placed at the center of CAESAR. The charged particles are bent by the Sweeper magnet into a series of charged particle detectors.

assume the momentum acceptance does not change between feeding the ground or excited states for a particular reaction.

### III. RESULTS

#### A. Experimental relative cross sections

Relative cross sections to different final states for a given residual nucleus could be determined from the number of ob-

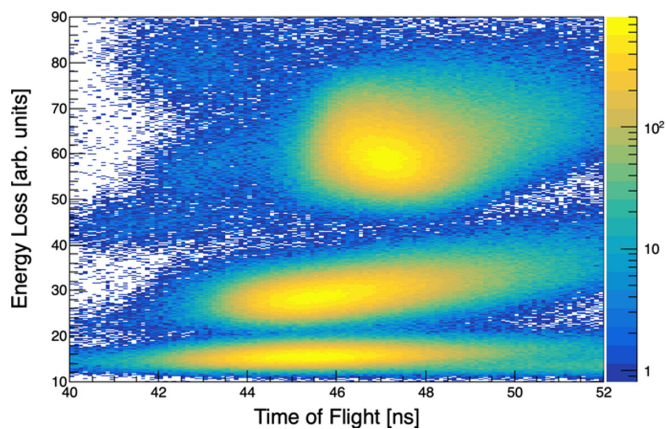


FIG. 2. The atomic number of a reaction product is determined on an event-by-event basis from the energy loss in the ionization chamber plotted against the time of flight from the target to the end of the focal plane. In this example the three bands correspond to beryllium (top), lithium (middle), and helium (bottom) isotopes from a  $^{10}\text{Be}$  beam. The color represents the number of counts.

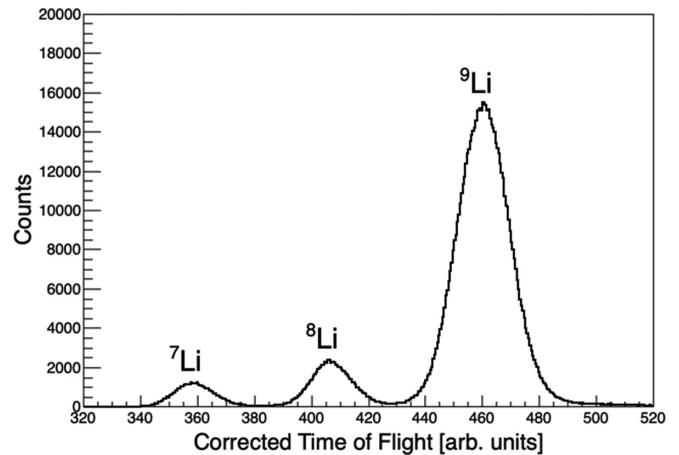


FIG. 3. Isotope separation for a given element shown from the corrected time of flight for reaction products passing through an element cut. This example shows the lithium isotopes:  $^7\text{Li}$ ,  $^8\text{Li}$ , and  $^9\text{Li}$  (left to right), produced from the  $^{10}\text{Be}$  beam.

served  $\gamma$  rays. The background observed in all  $\gamma$ -ray spectra was modeled by a double-exponential function. This shape was determined from the data collected in the ( $^7\text{Li}$ ,  $^6\text{He}$ ) reaction, since  $^6\text{He}$  has no bound excited states. Because the  $\gamma$  rays of interest are mixed with this background and CAESAR has an energy dependent efficiency, it was necessary to perform Monte Carlo simulations which take into account the detector geometry, resolution, acceptance, and efficiency. GEANT4 simulations, which model the in-beam response of CAESAR after Doppler reconstruction, were performed for the observed  $\gamma$ -ray transitions. These simulations were benchmarked against laboratory-frame  $\gamma$ -ray spectra from calibration sources. The in-beam simulations were combined with the background shape and scaled to match the experimental spectra. The number of simulated events necessary to reproduce the experimental spectra, multiplied by the scaling factor provides the number of decays. This number divided by the number of charged particles which triggered the system gives, in turn,

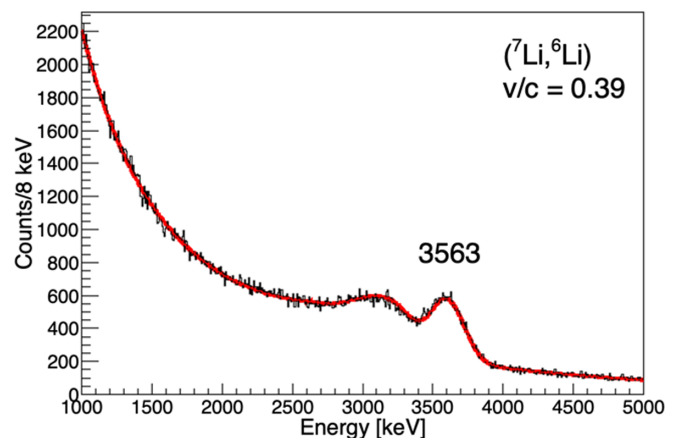
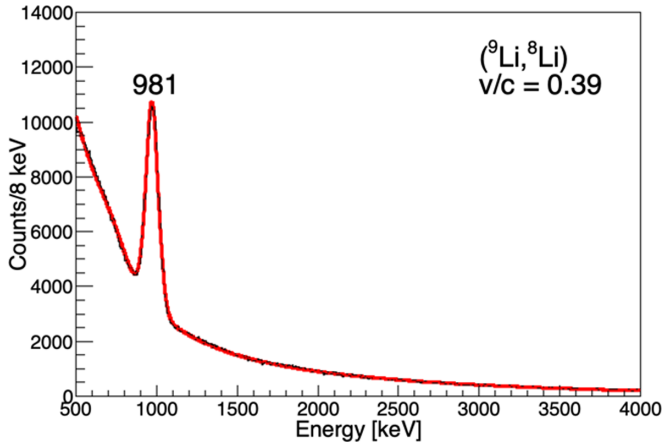


FIG. 4. Doppler-corrected energy spectrum for  $^6\text{Li}$ . The data are shown in black with the best fit, consisting of a GEANT4 simulation plus a double exponential background, shown in red.

FIG. 5. Same as Fig. 4 for  ${}^8\text{Li}$ .

the partial cross section to the corresponding final state. The relative cross section to the ground state corresponds to events without  $\gamma$  decays from the residue, and is given by the remainder necessary to complete the total inclusive cross section,  $\sigma_{\text{g.s.}} = \sigma_{\text{inc}} - \sigma_{\text{ex}}$ .

The CAESAR data from the  $({}^7\text{Li}, {}^6\text{Li})$  reaction is shown in Fig. 4 where the  $\gamma$  rays are in coincidence with the  ${}^6\text{Li}$  reaction products. The only observed transition is from the known  $0^+$  state at 3.56 MeV, the isobaric analog of the ground state of  ${}^6\text{He}$ , to the  $1^+$  ground state of  ${}^6\text{Li}$ . Although it is located above the  $Q(\alpha)$  energy of 1.47 MeV, this state decays exclusively via  $\gamma$  decay, unlike the  $3^+$  state at 2.19 MeV which undergoes  $\alpha + d$  dissociation. Analogous figures are shown for the  $({}^9\text{Li}, {}^8\text{Li})$  and  $({}^{10}\text{Be}, {}^9\text{Li})$  reactions in Figs. 5 and 6, respectively. The only transitions observed in  ${}^8\text{Li}$  and  ${}^9\text{Li}$  are from the 0.98 MeV  $1^+$  and the 2.69 MeV  $1/2^-$  states to the  ${}^8\text{Li}$  and  ${}^9\text{Li}$  ground states, respectively.

For the three reactions presented in this work, inclusive absolute cross section measurements at the same beam energy and target thickness have already been performed [19]. The absolute partial cross sections are then deduced using the relative cross sections determined from this work and the absolute inclusive cross sections measured in the previous work. The results are shown in Table II.

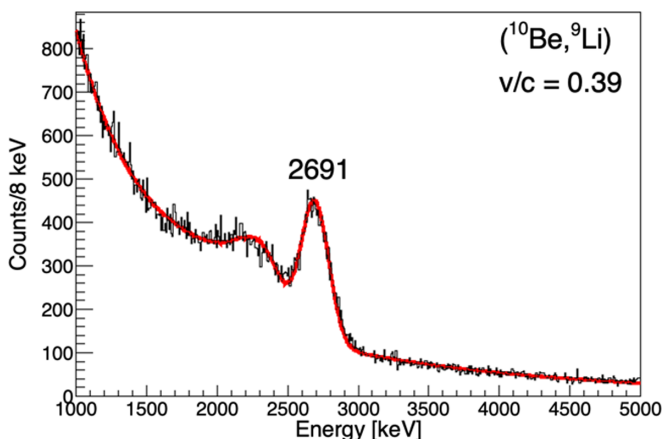
FIG. 6. Same as Fig. 4 for  ${}^9\text{Li}$ .

TABLE II. Reaction, spin-parities, excitation energies, and measured partial cross sections of the final states. The cross section for the ground states are determined by subtracting the partial cross sections for the excited states from the previously measured inclusive cross sections.

Reaction	$J^\pi$	$E_x$ [MeV]	$\sigma_{\text{par}}$ [mb]
$({}^7\text{Li}, {}^6\text{Li})$	$1^+$	-	26.1(18)
	$0^+$	3.56	4.6(4)
$({}^9\text{Li}, {}^8\text{Li})$	$2^+$	-	41.4(31)
	$1^+$	0.98	14.2(12)
$({}^{10}\text{Be}, {}^9\text{Li})$	$3/2^-$	-	22.6(13)
	$1/2^-$	2.69	3.4(3)

### B. Theoretical cross sections

The theoretical removal cross sections were calculated based on the tabulated, numerical overlap functions from the VMC calculations [20,21]. The procedure followed was that discussed in the earlier inclusive cross sections analysis of Ref. [19]. In summary, each tabulated VMC radial overlap, with single-particle quantum numbers  $\ell_j$ , was fitted by a bound Woods-Saxon potential eigenstate using the correct empirical separation energy for the chosen initial and final states. A best fit was achieved by adjusting the potential radius and diffuseness parameters ( $r_{\text{VMC}}$ ,  $a_{\text{VMC}}$ ) and the overall normalization of the calculated radial wave-function. In addition, the VMC densities of the residual nuclei were used in computing the residue-target nucleus optical potentials and their elastic  $S$  matrices, required by the reaction model [2]. The fitted Woods-Saxon radial form-factors provide a very good description of the VMC overlaps. An example, for the  $({}^{10}\text{Be} | {}^9\text{Li}^*(1/2^-) + p)$  transition, is shown in Fig. 7, that also shows the corresponding neutron and proton one-body densities of the  ${}^9\text{Li}$  residue.

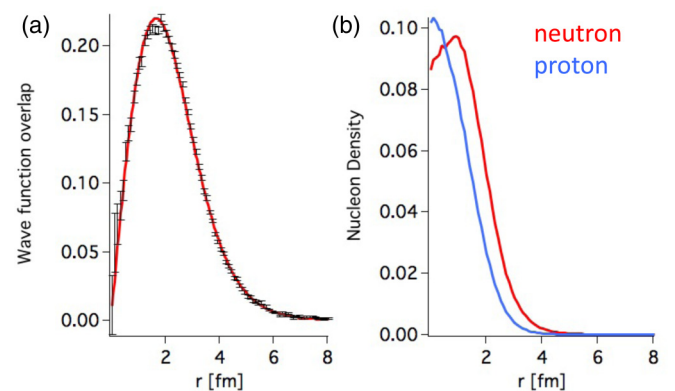


FIG. 7. (a) VMC radial overlap (points) for the  $({}^{10}\text{Be} | {}^9\text{Li}^*(1/2^-) + p)$  removal reaction. The fitted Woods-Saxon potential eigenstate is shown by the solid red curve. (b) VMC proton (blue) and neutron (red) one-body densities for the  ${}^9\text{Li}$  residual nucleus. The overlap plot is representative of the quality of fit for the other cases, as shown in Fig. 6 of Ref. [19].

TABLE III. The fitted Woods-Saxon potential radius and diffuseness parameters, the VMC spectroscopic factors and the theoretical partial cross sections for each removal reaction channel.

Reaction	$J^\pi$	$E_{\text{VMC}}^*$ [MeV]	$j$	$r_{\text{VMC}}$ [fm]	$a_{\text{VMC}}$ [fm]	SF <sub>VMC</sub>	$\sigma_{\text{VMC}}$ [mb]
( <sup>7</sup> Li, <sup>6</sup> He)	0 <sup>+</sup>		3/2	1.80(2)	0.69(2)	0.389	21.8(5)
( <sup>7</sup> Li, <sup>6</sup> Li)	1 <sup>+</sup>		1/2	1.90(3)	0.58(5)	0.246	13.9(6)
			3/2	1.79(3)	0.59(4)	0.436	25.0(9)
	0 <sup>+</sup>	4.0	3/2	1.80(2)	0.71(5)	0.192	10.1(7)
( <sup>9</sup> Li, <sup>8</sup> Li)	2 <sup>+</sup>		1/2	1.66(2)	0.33(4)	0.039	1.92(7)
			3/2	1.37(1)	0.42(1)	0.926	43.1(7)
	1 <sup>+</sup>	0.8	1/2	1.65(1)	0.13(3)	0.023	0.96(2)
			3/2	1.36(1)	0.53(1)	0.440	20.0(3)
( <sup>10</sup> Be, <sup>9</sup> Li)	3/2 <sup>-</sup>		3/2	1.47(2)	0.92(4)	1.174	40.7(8)
	1/2 <sup>-</sup>	1.2	1/2	1.55(1)	0.92(1)	0.444	19.4(1)

The calculated theoretical partial cross sections<sup>1</sup> are shown in Table III. For each reaction and final state we also show the spectroscopic factor (the norm of the VMC overlap function) since this is indicative of the overall strength of the transition. We note that updated VMC calculations [20,21] have been reported subsequent to the publication of references [10,19]. So, the present work involves updated fits to these revised VMC inputs. While the details of the Woods-Saxon parameters  $r_{\text{VMC}}$  and  $a_{\text{VMC}}$  from the fits in this work are different to those in Refs. [10,19], the resulting cross sections do not change significantly.

#### IV. DISCUSSION

The purpose of this study is to compare experimental cross sections between mirror reactions, going from analog states of both the initial and final nuclei. Since the nuclear force is charge-independent, the theoretically calculated single-nucleon overlaps and associated spectroscopic factors for these mirror reactions are identical in the absence of the Coulomb interaction. Unlike heavier systems, where the required nuclear structure input to the reaction model is usually taken from truncated shell-model calculations, VMC many-body calculations are available for *p*-shell nuclei. The VMC wave functions used here are based on the Argonne  $v_{18}$  [22] and Urbana X [23] two- and three-body interactions, and treat the effects of short- and long-range correlations with no explicit truncation of the basis of available configurations. Thus, comparisons of the measured and calculated cross sections for these mirror systems should provide useful probes of these combined wave functions and reaction model calculations.

It should be noted that the  $A = 7$  to  $A = 6$  reactions, based on the proton and neutron removal from <sup>7</sup>Li are not actually a mirror case, because of the different number of protons and neutrons in the respective  $p_{3/2}$  shells in <sup>7</sup>Li, and therefore the different parentages between the ground state of <sup>7</sup>Li and the <sup>6</sup>He(0<sup>+</sup>) and <sup>6</sup>Li(0<sup>+</sup>) analog states. This difference is appar-

ent in the VMC spectroscopic factors displayed in Table III, showing nearly a factor of two between them.

In the following the experimental partial cross sections within each mirror pair is compared to the theoretical values. The results are collected in Table IV, where the measured and calculated partial cross sections are shown. The sixth column also shows the ratio of these cross sections to aid their comparison. These ratios are also plotted in Fig. 8 as a function of the asymmetry energy  $\Delta S$  which reflects the difference between the proton and neutron separation energies, as explained in [3,4].

The VMC wave functions calculated using two- and three-nucleon forces, compute densities, overlaps, and

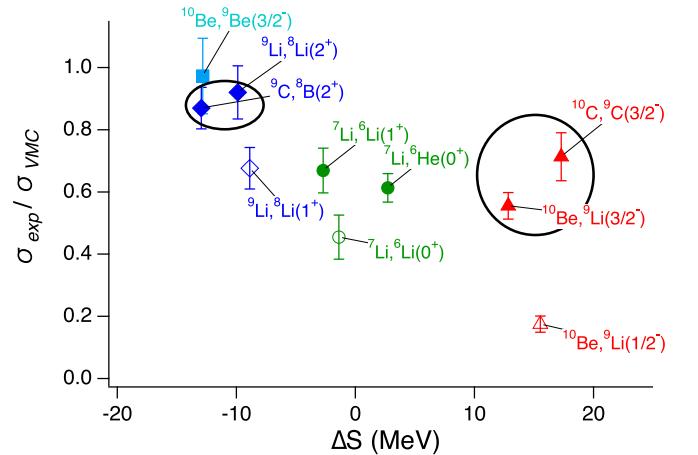


FIG. 8. Ratios of experimental cross section to VMC cross section shown in Table IV as a function of the asymmetry energy  $\Delta S = S_n - S_p$  for neutron removal and  $S_p - S_n$  for proton removal. The blue diamonds correspond to the  $A = 9$  to  $A = 8$  mirror pair, the green circles to the  $A = 7$  to  $A = 6$  case, and the red triangles to the  $A = 10$  to  $A = 9$  mirror pair. The light blue square shows the result for the one neutron removal from <sup>10</sup>Be [10]. The data points corresponding to the two mirror pairs are grouped together with black ellipses. The open symbols denote the results obtained for excited states as the final states, which clearly show a different trend than the ground states. Note that the cross section ratios displayed here are not to be compared with the reduction factors displayed in [3,4], which are based on different experimental values and structure models (see text).

<sup>1</sup>In practice, the cross sections are calculated using a normalized radial overlap, computed from the best-fit Woods-Saxon geometry. This cross section is then scaled by the norm of the original VMC overlap, the spectroscopic factor for the given transition.

TABLE IV. Comparison of the experimental and theoretical partial cross sections for the various mirror reactions. Except for the  $A = 7$  to  $A = 6$  case, the first two rows of each group show the direct mirror comparison. Other rows show the results for other final states. The last row contains the previous result [10] on neutron removal from  $^{10}\text{Be}$ .

Reaction	Final state	$E^*$ [MeV]	$\sigma_{\text{exp}}$ [mb]	$\sigma_{\text{VMC}}$ [mb]	$\sigma_{\text{exp}}/\sigma_{\text{VMC}}$	$B_{\text{removal}}$ [MeV]	$B_{\text{core}}$ [MeV]
$(^7\text{Li}, ^6\text{He})$	$0^+$	0	13.4(7) <sup>a</sup>	21.8(5)	0.61(5)	9.97	0.97
$(^7\text{Li}, ^6\text{Li})$	$0^+$	3.56	4.6(4) <sup>b</sup>	10.1(7)	0.45(7)	10.81	0.14
	$1^+$	0	26.1(18) <sup>b</sup>	39.0(15)	0.67(7)	7.25	1.47
$(^9\text{C}, ^8\text{B})$	$2^+$	0	56(3) <sup>c</sup>	64.4(15) <sup>a</sup>	0.87(7)	1.3	0.14
$(^9\text{Li}, ^8\text{Li})$	$2^+$	0	41.4(31) <sup>b</sup>	45.0(8)	0.92(9)	4.06	2.03
	$1^+$	0.98	14.2(12) <sup>b</sup>	21.0(3)	0.68(7)	5.04	1.05
$(^{10}\text{C}, ^9\text{C})$	$3/2^-$	0	23.4(11) <sup>d</sup>	32.8(20) <sup>d</sup>	0.71(8)	21.28	1.3
$(^{10}\text{Be}, ^9\text{Li})$	$3/2^-$	0	22.6(13) <sup>b</sup>	40.7(8)	0.55(5)	19.64	4.06
	$1/2^-$	2.69	3.4(3) <sup>b</sup>	19.4(12)	0.18(3)	22.33	1.37
$(^{10}\text{Be}, ^9\text{Be})$	$3/2^-$	0	71(4) <sup>d</sup>	73(5) <sup>d</sup>	0.97(12)	6.81	1.66

<sup>a</sup>Taken from [19].

<sup>b</sup>Uses the relative cross section from the present work combined with the inclusive cross section of [19].

<sup>c</sup>Taken from [8].

<sup>d</sup>Taken from [10].

spectroscopic factors in a consistent way, taking into account correlations between nucleons. So, the use of the VMC results in the calculations of the single-particle cross sections is an attempt to describe the reaction and the structure parts of the theoretical cross section in the most self-consistent way. It should be noted that the comparison made here is unlike comparisons with theoretical cross sections based on shell model spectroscopic factors and Hartree-Fock densities where a reduction trend with asymmetry energy is now well established [3,4]. The present comparison is made of partial cross sections to individual final states, and not of inclusive cross sections that include all bound final states of the residue. The ratios obtained between the experimental and theoretical partial cross sections should not therefore be directly compared with those in the reduction factor plot of [3,4]. Rather, the aim of this comparison is to explore and quantify the level of discrepancy brought by the approach and approximations made in the calculation of the theoretical cross sections combining the VMC structure results with the eikonal reaction model.

Although the reactions going from  $^7\text{Li}(3/2^-)$  to  $^6\text{He}(0^+)$  and  $^6\text{Li}(0^+)$  are not mirrored, they are interesting to compare because of the nature of the final states. On the proton removal side the  $^6\text{He}(0^+)$  residue has a well-known two-neutron halo structure, and its analog state on the neutron removal side  $^6\text{Li}(0^+; T = 1)$  has a very similar structure [24] with a halo composed of a neutron and a proton. The binding energies  $B_{\text{core}}$  of the two final states are both smaller than the nucleon removal energies  $B_{\text{removal}}$  by an order of magnitude or more, with the smallest  $B_{\text{core}}$  for the  $^6\text{Li}(0^+)$  final state. At first glance, one would conclude that the smaller reduction factor observed for this latter state originates from the weaker binding of the  $^6\text{Li}(0^+)$  core, and that the halo nature of this state plays a role in its survival probability. However, building upon earlier analyses [25–28] of reaction cross section calculations of very weakly-bound systems, a calculation including the breakup degree of freedom of a weakly bound core (see Supplemental Material [29]) shows that this weak binding has a negligible effect on the calculation of the single-particle nu-

cleon removal cross sections. From a reaction dynamics point of view, the two reactions are therefore very similar—with nearly identical  $\Delta S$  values—and the difference should be attributed to a structural effect. Note that the cross-sections ratio for the  $^6\text{Li}(1^+; T = 0)$  ground state is consistent within error bars with that of the  $^6\text{He}(0^+)$  ground state.

The first mirror pair case ( $^9\text{C}(3/2^-)$ ,  $^8\text{B}(2^+)$ ) and ( $^9\text{Li}(3/2^-)$ ,  $^8\text{Li}(2^+)$ ) shows i) a consistent result within error bars between the two members, and ii) a much closer agreement with the theoretical predictions. The latter could be attributed to the low  $B_{\text{removal}}$  energies, and is in line with the more general observation that the theoretical cross sections are closer to the experimental ones for the removal of weakly bound nucleons. This is clearly illustrated in Fig. 8, where the ratios closer to 1 lie on the negative  $\Delta S$  side of the plot. The average value of the ratio for this pair is 0.90(11). Comparing to the previous case on  $^7\text{Li}$  neutron removal, it is interesting to note that the  $B_{\text{core}}$  energy of  $^8\text{B}(2^+)$  is the same as  $^6\text{Li}(0^+)$ , but the  $B_{\text{removal}}$  energies vary by almost an order of magnitude between the two reaction channels. This observation supports the model calculations, presented in the Supplemental Material [29] that a weak binding of the core has little effect on the dynamics of the reaction, as commented earlier, but that the binding energy of the removed nucleon plays a more significant role. Unlike in the comparisons made in [3,4] however, the possible dependency of the reduction factor to missing correlations in the wave functions is removed in this case, since the VMC wave functions should include the major part of these correlations. The data point for the ( $^{10}\text{Be}$ ,  $^9\text{Be}(3/2^-)$ ) from [10] has been added as another example where the cross-sections ratio is compatible with 1. Similarly to the previous  $A = 7$  to  $A = 6$  case, the ratio obtained when the final state is an excited state appears smaller than for the ground state, even though both the  $B_{\text{removal}}$  and  $B_{\text{core}}$  energies are within 1 MeV between the two final states. As will be shown below, this trend is further reinforced when looking at well-bound nucleon removal.

The results from the second mirror pair ( $^{10}\text{Be}(0^+)$ ,  $^9\text{Li}(3/2^-)$ ) and ( $^{10}\text{C}(0^+)$ ,  $^9\text{C}(3/2^-)$ ) studied in

this work show a close to consistent result in the ratio between experimental and theoretical cross sections. In this case a deeply bound valence nucleon is removed in the reactions, with  $B_{\text{removal}}$  energies close to 20 MeV. The average ratio between the two members of the pair is 0.63(9), significantly smaller than the previous case. However, it should be noted that this suppression is not as pronounced as in the reduction factor plot based on shell-model structure input and inclusive cross sections [3,4], in which reduction factors around 0.3(1) are found at similar  $\Delta S$  values. However, the smallest ratio of 0.18(3) is observed once again for the population of the  ${}^9\text{Li}(1/2^-)$  excited state, even though little difference is expected in the dynamics of the reaction with respect to the population of the  ${}^9\text{Li}$  ground state.

Taking a broader look at the results presented in Fig. 8, it appears that two separate trends can be distinguished: one for the population of the ground states, and another for the population of the excited states. The trend observed for the ground states (solid symbols in the figure) is not as pronounced as in [3,4], which could indicate that the effects of short and long range correlations do vary as a function of the binding energy of the removed nucleon, assuming they are realistically described in the VMC wave functions. The deviation from unity when removing well-bound nucleons would then originate in missing mechanisms in the reaction model. The trend for excited states (open symbols in the figure) is much more pronounced. This is a surprising result that cannot be readily attributed to the reaction dynamics. It should be noted that the spectroscopic factors obtained from the VMC calculations for these excited states differ significantly from those of traditional shell model calculations using appropriate effective interactions and model spaces. For instance, variations close to a factor of 3 can be found for the ( ${}^{10}\text{Be}$ ,  ${}^9\text{Li}(1/2^-)$ ) case [30], whereas the range of values for the ground state is much smaller. These observations could point to deficiencies in the VMC wave functions that would explain the significantly different trend. Indeed, a comparison between the VMC-calculated excited state energies (shown in Table III) and the experimental values (shown in Table IV) reveals a possible correlation between the trend of the excitation energies deviation and that of the cross section ratios.

## V. CONCLUSION

A set of single nucleon removal reactions was performed and their relative cross sections to final states were measured

using  $\gamma$  rays detected in coincidence with the residues. These relative cross sections combined with the previously measured absolute inclusive cross sections allowed absolute partial cross sections to be determined. Combining these new results, a set of reactions going from or to analog states could be assembled, with varying binding energies of the removed nucleons as well as the residues. These reactions are then compared to theoretical cross sections calculated from updated VMC calculations. In these calculations, VMC overlaps and densities are used as input into the eikonal model used to calculate the single-particle cross sections, producing the most consistent prediction of the experimental cross sections. These predictions could be used to explore the effects of binding on the calculations of theoretical cross sections using the eikonal model based on VMC input. The results indicate that the predicted cross sections match the measured ones the best for cases where the removed nucleon is weakly bound, but differ more significantly in cases where it is well bound. Two different trends are observed depending on whether the final states are a ground or excited state. This surprising behavior likely indicates deficiencies in the structure calculations of the excited states, as this discrepancy cannot be explained by differences in the reaction mechanism of the nucleon removal process. The better agreement observed for the ground states, as compared to the trend observed on inclusive cross sections and shell-model spectroscopic factors, seem to indicate that the effect of short and long range correlations between nucleons varies with binding. Further studies involving other mirror reaction cases are clearly needed to elucidate the observed behavior.

## ACKNOWLEDGMENTS

The authors would like to thank the NSCL staff for providing the multiple beams used in this experiment. This work is supported in part by the U. S. National Science Foundation under Grants No. 1102511 (NSCL), No. 2011398 (A.N.K.), No. 1306074 (P.D.Y.), and the U. S. Department of Energy, Office of Science, Office of Nuclear Physics under Grant No. DE-SC0020451 (D.B., A.G.), DOE Grant No. DE-AC05-06CH11357 (R.B.W.). R.B.W. acknowledges the support of the NUCLEI SciDAC project and Argonne's Laboratory Computing Resource Center. J.A.T. acknowledges the support of the United Kingdom Science and Technology Facilities Council (STFC) Grant No. ST/F005314/1.

- 
- [1] T. Aumann, C. Barbieri, D. Bazin, C. Bertulani, A. Bonaccorso, W. Dickhoff, A. Gade, M. Gómez-Ramos, B. Kay, A. Moro, T. Nakamura, A. Obertelli, K. Ogata, S. Paschalis, and T. Uesaka, *Prog. Part. Nucl. Phys.* **118**, 103847 (2021).
- [2] P. G. Hansen and J. A. Tostevin, *Annu. Rev. Nucl. Part. Sci.* **53**, 219 (2003).
- [3] J. A. Tostevin and A. Gade, *Phys. Rev. C* **90**, 057602 (2014).
- [4] J. A. Tostevin and A. Gade, *Phys. Rev. C* **103**, 054610 (2021).
- [5] Y. X. Zhao, Y. Z. Sun, S. T. Wang, Z. Y. Sun, X. H. Zhang, D. Yan, D. Y. Pang, P. Ma, Y. H. Yu, K. Yue, S. W. Tang, S. M. Wang, F. Fang, Y. Sun, Z. H. Cheng, X. M. Liu, H. R. Yang, C. G. Lu, and L. M. Duan, *Phys. Rev. C* **100**, 044609 (2019).
- [6] Y. Z. Sun, S. T. Wang, Z. Y. Sun, X. H. Zhang, S. Y. Jin, Y. X. Zhao, D. Y. Pang, S. W. Tang, D. Yan, P. Ma, Y. H. Yu, K. Yue, F. Fang, Y. J. Zhang, C. G. Lu, and L. M. Duan, *Phys. Rev. C* **104**, 014310 (2021).
- [7] D. L. Olson, B. L. Berman, D. E. Greiner, H. H. Heckman, P. J. Lindstrom, and H. J. Crawford, *Phys. Rev. C* **28**, 1602 (1983).
- [8] D. Bazin, R. J. Charity, R. T. de Souza, M. A. Famiano, A. Gade, V. Henzl, D. Henzlova, S. Hudan, H. C. Lee, S. Lukyanov, W. G. Lynch, S. McDaniel, M. Mocko, A. Obertelli,

- A. M. Rogers, L. G. Sobotka, J. R. Terry, J. A. Tostevin, M. B. Tsang, and M. S. Wallace, *Phys. Rev. Lett.* **102**, 232501 (2009).
- [9] K. Wimmer, D. Bazin, A. Gade, J. A. Tostevin, T. Baugher, Z. Chajecski, D. Coupland, M. A. Famiano, T. K. Ghosh, G. F. Grinyer, M. E. Howard, M. Kilburn, W. G. Lynch, B. Manning, K. Meierbachtol, P. Quarterman, A. Ratkiewicz, A. Sanetullaev, R. H. Showalter, S. R. Stroberg *et al.*, *Phys. Rev. C* **90**, 064615 (2014).
- [10] G. F. Grinyer, D. Bazin, A. Gade, J. A. Tostevin, P. Adrich, M. D. Bowen, B. A. Brown, C. M. Campbell, J. M. Cook, T. Glasmacher, S. McDaniel, P. Navrátil, A. Obertelli, S. Quaglioni, K. Siwek, J. R. Terry, D. Weisshaar, and R. B. Wiringa, *Phys. Rev. Lett.* **106**, 162502 (2011).
- [11] B. S. Pudliner, V. R. Pandharipande, J. Carlson, S. C. Pieper, and R. B. Wiringa, *Phys. Rev. C* **56**, 1720 (1997).
- [12] S. C. Pieper, K. Varga, and R. B. Wiringa, *Phys. Rev. C* **66**, 044310 (2002).
- [13] R. B. Wiringa, S. C. Pieper, J. Carlson, and V. R. Pandharipande, *Phys. Rev. C* **62**, 014001 (2000).
- [14] R. Yajzey, M. Bentley, E. Simpson, T. Haylett, S. Uthayakumar, D. Bazin, J. Belarge, P. Bender, P. Davies, B. Elman, A. Gade, H. Iwasaki, D. Kahl, N. Kobayashi, S. Lenzi, B. Longfellow, S. Lonsdale, E. Lunderberg, L. Morris, D. Napoli *et al.*, *Phys. Lett. B* **823**, 136757 (2021).
- [15] A. Gade and B. M. Sherrill, *Phys. Scripta* **91**, 053003 (2016).
- [16] D. Morrissey, B. Sherrill, M. Steiner, A. Stolz, and I. Wiedenhoever, *Nucl. Instrum. Methods Phys. Res. B* **204**, 90 (2003); 14th International Conference on Electromagnetic Isotope Separators and Techniques Related to their Applications.
- [17] D. Weisshaar, A. Gade, T. Glasmacher, G. Grinyer, D. Bazin, P. Adrich, T. Baugher, J. Cook, C. Diget, S. McDaniel, A. Ratkiewicz, K. Siwek, and K. Walsh, *Nucl. Instrum. Methods Phys. Res. A* **624**, 615 (2010).
- [18] M. D. Bird, S. J. Kenney, J. Toth, H. W. Weijers, J. C. DeKamp, M. Thoennessen, and A. F. Zeller, *IEEE Trans. Appl. Supercond.* **15**, 1252 (2005).
- [19] G. F. Grinyer, D. Bazin, A. Gade, J. A. Tostevin, P. Adrich, M. D. Bowen, B. A. Brown, C. M. Campbell, J. M. Cook, T. Glasmacher, S. McDaniel, A. Obertelli, K. Siwek, J. R. Terry, D. Weisshaar, and R. B. Wiringa, *Phys. Rev. C* **86**, 024315 (2012).
- [20] R. B. Wiringa, VMC spectroscopic overlaps, <https://www.phy.anl.gov/theory/research/overlaps/> (2020), updated: 2020-05-03
- [21] I. Brida, S. C. Pieper, and R. B. Wiringa, *Phys. Rev. C* **84**, 024319 (2011).
- [22] R. B. Wiringa, V. G. J. Stoks, and R. Schiavilla, *Phys. Rev. C* **51**, 38 (1995).
- [23] B. S. Pudliner, V. R. Pandharipande, J. Carlson, and R. B. Wiringa, *Phys. Rev. Lett.* **74**, 4396 (1995).
- [24] K. Arai, Y. Suzuki, and K. Varga, *Phys. Rev. C* **51**, 2488 (1995).
- [25] J. S. Al-Khalili and J. A. Tostevin, *Phys. Rev. Lett.* **76**, 3903 (1996).
- [26] J. S. Al-Khalili, J. A. Tostevin, and I. J. Thompson, *Phys. Rev. C* **54**, 1843 (1996).
- [27] R. C. Johnson and C. J. Goebel, *Phys. Rev. C* **62**, 027603 (2000).
- [28] J. Tostevin, R. Johnson, and J. Al-Khalili, *Nucl. Phys. A* **630**, 340 (1998).
- [29] See Supplemental Material at <http://link.aps.org/supplemental/10.1103/PhysRevC.105.034314> for a discussion of removal cross sections for reactions leading to weakly bound residual nuclei.
- [30] N. K. Timofeyuk, *Phys. Rev. C* **88**, 044315 (2013).